Conformer Lifetimes of Ethyl Cyanoformate from Exchange-Averaged Rotational Spectra

Nancy S. True

Department of Chemistry, University of California, Davis, Davis California 95616

Received: March 23, 2009; Revised Manuscript Received: May 7, 2009

Ethyl cyanoformate exists as a mixture of two conformers but displays three R-branch *a*-type band series in its rotational spectrum. Simulations with population fractions 0.37 at 210 K and 0.70 at 297 K undergoing conformer exchange with average conformer lifetimes, $\langle\tau_{iso}\rangle$, shorter than ~40 ps at ~210 K and shorter than ~37 ps at 297 K reproduce the experimental spectra between 26.5 and 38 GHz, the exchanging species accounting for the third set of bands. The upper-limit $\langle\tau_{iso}\rangle$'s are 1 order of magnitude longer than RRKM theory predictions and the population fractions are consistent with the total population with energy above 700 cm^{-1}, approximately twice the conformer interconversion barrier height. Model calculations indicate that extensive *K*-sublevel mixing in individual molecular eigenstates can produce the large population and the narrow distribution of the rotational-constant sum, $B + C$, consistent with the observed exchange-averaged band series.

Introduction

Rotational spectra obtained using cw acquisition methods provide unique information about low-barrier conformer exchange processes in thermally equilibrated samples under essentially collisionless conditions. Intense exchange-averaged *a*-type rotational band series produced by nearly prolate molecules with subnanosecond conformer lifetimes, at least 3 orders of magnitude shorter than the time between collisions at pressures required for spectral acquisition, are present in many rotational spectra.[1−3] Band frequencies and shapes provide information about conformer lifetimes and exchange-averaged rotational constants of thermal distributions of molecules with fixed energy and angular momentum. Relative-intensity measurements provide the fraction of molecules producing the exchange-averaged bands and its temperature dependence. The thermal average energy specific rate constants, $\langle k(E,J)\rangle$'s, obtained from analysis of exchange-averaged rotational bands are directly comparable to quantum statistical calculations and complement recent condensed phase 2D-IR studies of fast conformer exchange[4] and studies of conformational exchange of single eigenstates studied over narrow energy ranges.[5]

A conformationally averaged band series is present in rotational spectra of ethyl cyanoformate (ECF, $NCC(O)OCH_2$-CH_3).[1] An ensemble average conformer exchange rate constant, $\langle k(E)\rangle$ of ~25 GHz (average conformer lifetime, $\langle\tau_{iso}\rangle$ = ~40 ps) for the $J + 1 \leftarrow J = 8 \leftarrow 7$ transition of ECF was determined and a simple model for simulating the exchange-averaged band was also presented. In the present article, the $J + 1 \leftarrow J = 10 \leftarrow 9$, $11 \leftarrow 10$, $12 \leftarrow 11$, and $13 \leftarrow 12$ transitions of ECF at 210 and 297 K are compared with simulations and the factors contributing to band widths that arise from conformer exchange of a thermal distribution of molecules at fixed energies and low state densities are explored. Results for several $J + 1 \leftarrow J$ transitions provide information about the importance of total angular momentum on the conformer exchange process. Exchange-averaged bands of ECF are motionally narrowed with widths approximately twice those of the corresponding conformer bands. This indicates that $\langle\tau_{iso}\rangle$ for ECF is much shorter than the spectral time scale, τ_{sp}, (i.e., the reciprocal of the frequency difference between the same $J + 1 \leftarrow J$ transitions of the two conformers, ~400−500 ps)[1]) and both $\langle\tau_{iso}\rangle$ and the thermal distribution of exchange-averaged rotational constants in the sample can, in principle, contribute significantly to the observed band widths. It is possible to determine upper limits for $\langle\tau_{iso}\rangle$ and for the distribution of the rotational-constant sum, $B + C$, of the molecules producing the exchange-averaged (EA) series upper-limit $\langle\tau_{iso}\rangle$'s for ECF are compared with predictions based on quantum statistical RRKM theory. The upper limit of the distribution of the rotational-constant sum, $B + C$, which depends on the compositional variability of the molecular eigenstates that produce the EA bands is reported and compared to models. The relationship between the $B + C$ distribution and conformer exchange dynamics at fixed energy is developed in the following paragraphs.

ECF molecules undergoing conformer exchange at fixed energies exist in eigenstates with mixed conformational character. Pate et. al have described the rotational spectra of structurally mixed eigenstates that can be represented as linear combinations of zero-order conformationally localized and delocalized rovibrational basis states that have different rotational constants.[5−8] Basis states close in energy and with the same total angular momentum are coupled through Coriolis and/or anharmonic terms in the full molecular Hamiltonian to form molecular eigenstates. Random matrix calculations show that at high state densities and with large coupling interactions the composition of each molecular eigenstate mirrors the distribution of the zero-order states in the ensemble.[6,7] This statistical model is appropriate when a narrow energy range at high state densities is probed. For ECF, however, the EA series is produced by a thermal distribution of molecules at fixed internal energies, which span a range of several thousand cm^{-1} at 297 K.[1] The vibrational state density of ECF is only ~1/cm^{-1} near the conformer exchange barrier. A large fraction of the population with energy above the conformer exchange barrier is in an energy range where the vibrational state density is low and mechanisms for efficient state mixing may not present. Molecular eigenstates at energies where state densities are low may not have mixed conformational compositions or the percentages of different conformationally localized states forming them may vary over wide ranges. Variations in composition of the

10.1021/jp902619k CCC: $40.75
Published on Web 05/29/2009

molecular eigenstates will lead to a large distribution of exchange-averaged rotational constants and conformer lifetimes in a thermal sample. This article will refer to sets of coupled zero-order states as exchange networks to emphasize their time-dependent properties. The nature of the zero-order rovibrational states and the coupling constants among them determine the dynamics of each exchange network, the time evolution of its rotational constants, its average conformer lifetimes, and its averaged rotational constants.

Exchange averaging and its effects on transition lineshapes have been extensively addressed in general[9] and in the context of rotational,[5−8] infrared,[10] and magnetic resonance spectra.[11,12] The qualitative effects of conformer exchange on the thermal rotational spectrum of ECF are briefly outlined here. ECF is a nearly prolate polar asymmetric top and produces R-branch *a*-type rotational band series at frequencies that obey the relationship $\nu = \sim(B + C)(J + 1)$.[13] Each band is composed of clusters of *K*-sublevel transitions, $J'_{K_p'K_o'} \leftarrow J''_{K_p''K_o''}$, with selection rules: $J' = J'' + 1$, $K_{p'} = K_{p''}$, $K_{o'} = K_{o''} + 1$.[14] The frequency dispersion of the *K*-sublevel transitions in each band depends on *J* and the molecule's asymmetry and is ∼50−150 MHz for the ECF band spectra reported in this article. The rotational-constant sum for the vibrational ground states of the syn-anti (SA) and syn-gauche (SG) conformers of ECF, $B_0 + C_0$, are 2736.83 and 2956.17 MHz, respectively. Consequently, τ_{sp}, ($\tau_{sp} = \sim((J + 1)((B_0 + C_0)_{SG} - (B_0 + C_0)_{SA}))^{-1}$) ranges from ∼500 to ∼420 ps for the $J + 1 \leftarrow J = 10 \leftarrow 9$, $11 \leftarrow 10$, $12 \leftarrow 11$, and $13 \leftarrow 12$ rotational transitions studied in the present article. The lifetime of the conformationally localized zero-order states in an exchange network can be characterized by the time constant, τ_{iso} ($\tau_{iso} = (k_{SA\rightarrow} + k_{SG\rightarrow})^{-1} = k_{iso}^{-1}$). If $\tau_{iso} \gg \tau_{sp}$ (slow exchange) the zero-order conformationally localized rovibrational states produce distinct band series. Conformer exchange on the spectral time scale ($\tau_{iso} \sim \tau_{sp}$) produces changes in transition lineshapes similar to those observed in magnetic resonance spectra.[12] The exchange-averaged rotational *K*-sublevel transition frequencies and lineshapes are functions of the fraction of each type of zero-order state in the exchange network, the rotational constants, and transition dipole moments of the zero-order states, *J*, and τ_{iso}. Rotational transitions of molecules with exchange networks where $\tau_{iso} < \tau_{sp}$ (above coalescence) are exchange averaged and their width decreases as τ_{iso} becomes shorter. At the fast ($\tau_{iso} \ll \tau_{sp}$) exchange limit, the exchange-averaged *K*-sublevel transitions are not sensitive to τ_{iso} and at the experimental pressures employed their line width is determined by T_1 processes (collision induced rotational relaxation) and is ∼1 MHz. The frequencies and widths of the EA rotational bands produced at the fast-exchange limit depend on the exchange-averaged rotational constants and the associated frequency dispersion of the *K*-sublevel transitions. A thermal distribution of molecules spread over several thousand centimeters with a range of state densities that spans several orders of magnitude will have a distribution of exchange network compositions and exchange-averaged rotational constants, a range of τ_{iso}'s, and will produce a distribution of exchange-averaged lineshapes that add to produce exchange-averaged bands. Additionally, the thermal broadband microwave spectra of ECF were acquired with Stark-effect modulation and phase-sensitive detection and each transition has a set of associated Stark lobes.[14]

Bands of the EA series of ECF are intense and only a few hundred megahertz wide,[1] indicating that much of the population has similar exchange-averaged rotational constants. This requires the exchange networks of a large fraction of molecules to have similar fractional compositions of each type of zero-order state. Surprisingly, the vibrational state density of ECF is only ∼10/cm^{-1} at 1000 cm^{-1} (the average vibrational energy at 297 K) and the number and composition of the zero-order states contained in 1 cm^{-1} energy intervals (grains) near 1000 cm^{-1} vary widely. Any description of the thermally populated molecular eigenstates of ECF consistent with the EA band intensities and rotational-constant distribution requires large exchange networks and extensive state mixing at low internal energies. *K*-sublevel mixing that occurs via Coriolis interactions can increase the number of states comprising an exchange network at *E* and *J* by as much as $(2J + 1)$ and lower the threshold energy for producing a narrow distribution of fast-exchange-averaged rotational constants. Classical trajectory calculations show that nonaxial internal rotors promote extensive *K*-sublevel mixing in near-symmetric top molecules,[17] and torsion-rotation Coriolis coupling in molecules with nonaxial rotors causes extensive basis set mixing.[18] Experiments sensitive to *K*-sublevel mixing yield conflicting results, however. The survival probability for coherent excitation of the acetylenic C−H stretch in a series of halogen-substituted butynes (XCH_2-CH_2-CCH) that undergo gauche−trans conformer isomerization is consistent with *K*-state mixing.[19] The density of coupled states in the eigenstate resolved spectra agrees with calculated rovibrational state densities for 4-chlorobutyne and 4-bromobutane. For 4-fluorobutyne, however, the experimental increase of state densities with *J* deviates from the expected $2J + 1$ growth at high *J* suggesting incomplete *K*-sublevel mixing at higher *J*.[19] Modeling the degree of fine structure present in the high-resolution IR spectrum of the asymmetric stretch of 1-butene required complete mixing of all of the rovibrational states consistent with conservation of energy and total angular momentum.[20] Eigenstate resolved spectra of 2-fluoroethanol[21] and isobutene[22] and other medium sized molecules[6] are also consistent with fragmentation into states with different values of *K*. The extent of *K*-sublevel mixing in thermally populated exchange networks of ECF is explored in the present article by comparing the bandwidths and intensity of the EA series with predictions for two exchange network models.

Experimental Section

Sample preparation and spectral acquisition methods used to obtain the low-resolution spectra of ECF have been described previously.[1,15] Spectra recorded as functions of increasing and decreasing frequency were digitized at 0.5 MHz frequency increments. Band shapes and width observed in spectra at ∼210 and 293 K are independent of the scan direction but the frequencies of the band maxima differ by ∼50 MHz due to the 1s time constant and 10 MHz s^{-1} scan rate employed. The frequency axes of the experimental spectra shown in this article are offset by 25 MHz to make them directly comparable to simulated spectra based on high-resolution rotational constants.

Results

Low-Resolution Rotational Spectra of ECF. Low-resolution microwave spectra of ECF obtained between 26.5 and 38 GHz at 297 and 210 K are shown in part a of Figure 1 and part a of Figure 2a, respectively. The two R-branch *a*-type band series ($\nu = (B + C)(J + 1)$ with $B + C = 2752(2)$ MHz (bands at frequencies indicated by ←) and ∼2954(2) MHz (bands at frequencies indicated by →) are assigned to the SA and SG conformers, respectively.[15] The vibrational ground-state $B + C$ values of the SA and SG conformers determined from high-resolution assignments are 2736.83 and 2956.17 MHz, respec-

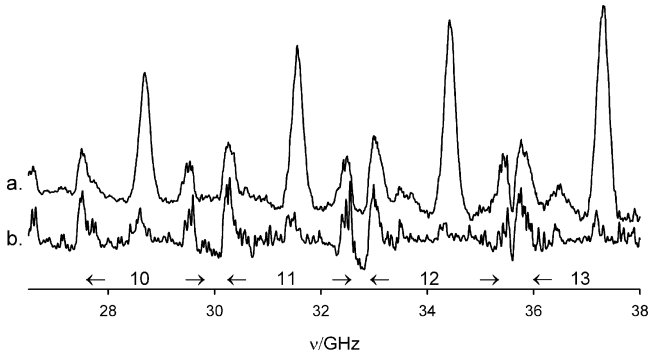

Figure 1. Stark-modulated rotational band spectrum of ethyl cyanoformate between 26.5 and 38 GHz at 297 K; a, experimental spectrum; b, slow-exchange ($\tau_{iso} \gg \tau_{sp}$) simulated spectrum. Sets of arrows (← J + 1 →) point to the $J + 1 \leftarrow J$ bands of the SA (←) and SG (→) conformers.

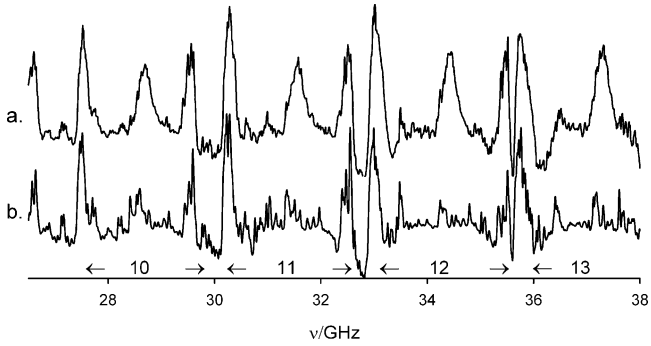

Figure 2. Stark-modulated rotational band spectrum of ethyl cyanoformate between 26.5 and 38 GHz at 210 K; a, experimental spectrum; b, slow-exchange ($\tau_{iso} \gg \tau_{sp}$) simulated spectrum. Sets of arrows (← J + 1 →) point to the $J + 1 \leftarrow J$ bands of the SA (←) and SG (→) conformers.

tively.[23] The difference between the corresponding high- and low-resolution $B + C$ values of the less prolate SA conformer (Ray's asymmetry parameter,[14] κ, is −0.899) occurs because most of the intense K sublevel transitions for each $J + 1 \leftarrow J$ transition occur at frequencies greater than $(B + C)(J + 1)$. The difference between the corresponding low- and high-resolution $B + C$ values of the more prolate SG conformer (κ = −0.947) is due to semiresolved vibrational satellite bands at lower frequencies from the ground-state pileups. The $J + 1$ = 10, 11, 12, and 13 bands of the SA conformer (band widths ∼150 MHz fwhm) are at 27 545 MHz, 30 290 MHz, 33 040, and 35 790 MHz. The $J + 1$ = 10, 11, and 12 bands of the SG conformer (band widths ∼150 MHz) are at 29 540 MHz, 32 480 MHz, and 35 445 MHz. Band frequencies, widths, and profiles of the SA and SG series are not significantly temperature dependent. Sets of arrows (← $J + 1$ →) point to SA (←) and SG (→) bands with the same value of $J + 1$. The frequency differences, $\nu_{SG} - \nu_{SA}$, for the $J + 1 \leftarrow J = 10 \leftarrow 9$, $11 \leftarrow 10$, $12 \leftarrow 11$, and $13 \leftarrow 12$ transitions are 1995, 2190, 2405, and 2695 MHz respectively and correspond to τ_{sp}'s for conformer exchange of 501, 457, 416, and 371 ps, respectively. The EA series obeys $\nu = (B + C)(J + 1)$ with a $B + C$ value of 2870 MHz at 210 K. Its estimated high-resolution $B + C$ value is 2863 MHz.[13,15] Bands of the EA series shift to higher frequency and are narrower at 297 K, as shown in Figure 3. The $J + 1$ = 10, 11, 12, and 13 bands of the EA series (observed Stark-modulated band widths ∼300 MHz at 210 K, and ∼250 MHz at 297 K) are at 28 700, 31 535, 34 435, and 37 330 MHz. The relative-intensity ratio in the Stark-modulated spectra, I_{SA}:I_{SG}:I_{EA} is ∼1:0.9:1 at 210 K and ∼1:0.9:3 at 297 K.

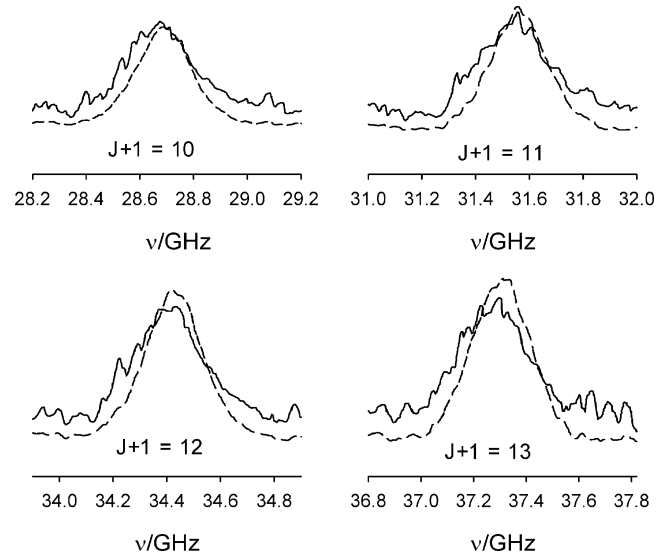

Figure 3. Overlay of the microwave spectra of the $J + 1 \leftarrow J = 10 \leftarrow 9$, $11 \leftarrow 10$, $12 \leftarrow 11$, and $13 \leftarrow 12$ transitions of the EA (exchange-averaged) band series of ECF at 210 K (solid lines) and 297 K (dashed line). The intensities of the bands at 297 are scaled to match those at 210 K.

Slow-Exchange Spectral Simulations. Simulated slow-exchange ($\tau_{iso} \gg \tau_{sp}$) spectra of ECF between 26.5 and 38 GHz at 297 and 210 K are shown in part b of Figure 1 and part b of 2, respectively. These simulations used the method described in ref 1, which is briefly summarized here. Vibrational excitation in the low-frequency O−ethyl torsional vibration produces large changes in the rotational constants of ECF. The levels of excitation in the other higher-frequency vibrations possible at 210 and 297 K produce much smaller changes in rotational constants and were not included in spectral simulations. The O−ethyl torsional dependence of the internal rotation constant and potential energy was calculated using the MP2/HF/6-311++G** theoretical model and fit to Fourier series. A 1D internal rotation Hamiltonian incorporating these terms was diagonalized in the free rotor basis. Figure 4 shows the O−ethyl potential function and associated eigenfunctions. The rotational constants A, B, and C, also determined using the MP2/HF/6-311++G** theoretical model, were fit to Fourier series and their expectation values were determined for each eigenfunction. Although the expectation values of the rotational constants for the ground states of the SA ($\langle A \rangle$ = 6453.96 MHz, $\langle B \rangle$ = 1500.06 MHz, $\langle C \rangle$ = 1237.31 MHz) and SG ($\langle A \rangle$ = 6811.14 MHz, $\langle B \rangle$ = 1556.23 MHz, $\langle C \rangle$ = 1406.25 MHz) conformers agree well with the experimental ground-state rotational constants,[23] using unscaled values of $\langle A \rangle$, $\langle B \rangle$, and $\langle C \rangle$ results in 60−80 MHz discrepancies in calculated transition frequencies between 26.5 and 38 GHz. Therefore, the calculated expectation values of the rotational constants of all of the localized SA and SG torsional states were multiplied by the appropriate scaling factors determined for their respective SA and SG ground states. The calculated expectation values of the rotational constants of all of the T (transition states, i.e. the three states directly below the SA−SG barrier and the three states directly above the SA−SG barrier, which have mixed conformer character) and the D states (delocalized states, i.e. the states above the T states but below the SG−SG barrier) were multiplied by the average values of the SA and SG scaling factors. Scaled rotational constants for the 1000 lowest energy states in the O−ethyl torsion were used to simulate the R-branch a-type ($J'_{K_p',K_o'} \leftarrow J''_{K_p'',K_o''}$) spectra shown in part b of Figure 1 and part b of Figure

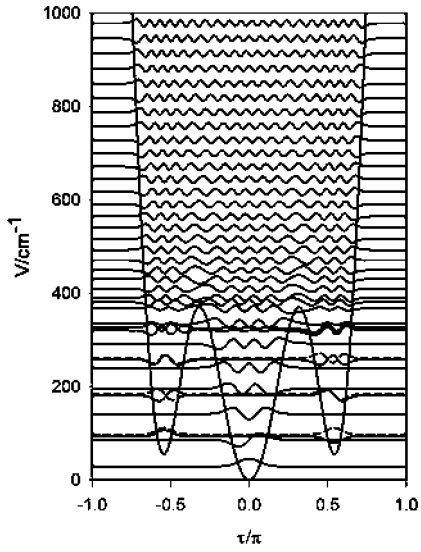

Figure 4. O−ethyl internal rotation potential function of ECF calculated using the MP2/HF/6-311++G** theoretical model. Eigenfunctions are plotted at the corresponding energy eigenvalues. The minimum at 0 corresponds to the SA conformer and minima near $\pm 0.5\pi$ correspond to the SG conformer.

2 using previously described methods.[1] The number of eigenfunctions included ensured that all of the torsional eigenstates with Boltzmann factors greater than 0.001 relative to the ground state were included in the simulations at both temperatures.

Spectra shown in part a of Figure 1 and part a of Figure 2 were obtained using Stark-effect modulation with a 3200 V/cm electric field and phase-sensitive detection. The zero-field signal is plotted upward. Spectra calculated at zero field and at 3200 V/cm were combined to produce the simulated spectra. The transitions with $K_p \geq 2$ were calculated using a first-order Stark effect with a second-order correction. The Stark shifts of the transitions with $K_p = 0$ and 1 that do not have a first-order Stark effect were calculated using a second-order Stark effect.[23,14] The experimentally determined *a*-axis dipole moment, μ_a, of the SA and SG conformers, 4.44 and 4.25 D, respectively[23] and the average value of μ_a for the T and D states were used in these calculations. A Lorentzian line shape function with a 5 MHz fwhm, truncated ±500 MHz from the center frequency, was applied to the zero-field transitions and Stark lobes. Intensities were calculated at 1 MHz frequency intervals. The much weaker *b*- and *c*-type spectra were not included in the simulation. The *b* axis dipole moment of both conformers is ∼0 and the *c* axis dipole moment of the SA and SG conformer is 0 and 1.08 D, respectively.[23]

The slow-exchange simulated spectra between 26.5 and 38 GHz at 297 and 210 K, shown in part b of Figure 1 and part b of Figure 2, reproduce the observed relative intensities of the SA and SG bands and bandwidths. The band shapes of the $J + 1 \leftarrow J$ transitions of the less prolate SA conformer are determined by the frequency dispersion of the *K*-sublevel transitions rather than the variation in the rotational constants of included torsionally excited states and are reproduced in the simulation. For the SA conformer of ECF the transitions, $J'_{K_p',K_o'} \leftarrow J''_{K_p'',K_o''}$, with $0 < K_p'' \leq 2$, and one transition with $K_p'' = 3$, fall outside the main pileups by more than 200 MHz for $J'' = 9-12$. The remaining transitions have a frequency dispersion of ∼100 for $J'' = 9$ and increase to 130 for $J'' = 12$. For the more prolate SG conformer only the transitions with $0 < K_p' \leq 2$ fall outside the main pileups. The other *K*-sublevel transitions have a frequency dispersion of ∼50 MHz for $J + 1 = 10$ increasing to ∼70 MHz for $J + 1 = 13$. The simulated band profiles of the more prolate SG conformer show resolved torsional satellite structures, whereas the experimental SG bands do not. This may be due to rapid exchange among states localized in the SG well compared to the spectral time scale for this process.[6−8] The spectral time scale for SG intrawell averaging, determined by the frequency differences among the SG O−ethyl torsional satellite bands, is 18 ns for $J + 1 = 10$ and 14 ns for $J + 1 = 13$. The SA and SG transitions with $K_p = 0$ and 1 are not apparent in the experimental spectra shown in part a of Figure 1 and part a of Figure 2. Simulations show that the groups of ground-state and vibrational satellite SA and SG transitions with $K_p = 0$ and 1 are largely canceled by their Stark lobes. The calculated second-order Stark shifts are between 7 and 70 MHz for the $J + 1 \leftarrow J = 10 \leftarrow 9$ transition for $K_p = 0$ and 1 and Stark shifts are smaller for the higher-frequency transitions.

Slow-exchange simulations do not reproduce the intense temperature-dependent EA band series. The regions between corresponding $J + 1 \leftarrow J$ SA and SG bands in the simulated slow-exchange spectra are dominated by transitions of the T states, which have a wide range of rotational constants, and the higher-energy D states, which have similar rotational constants.

Exchange-Averaged Spectral Simulations. Initially, the $J + 1 \leftarrow J = 10 \leftarrow 9$ EA band at 297 K was simulated using the Bloch model modified for chemical exchange described in ref 1 using both two- and three-site exchange mechanisms. The observed EA band is not sensitive to the exchange mechanism and several models can produce both the transition frequencies and widths required to simulate the EA bands. For both two- (SA, SG) and three-site (SA, SG, delocalized (D)) models, populations and rate constants were adjusted to produce the experimentally observed EA band frequencies and profiles. Two-site exchange using the SA and SG $J + 1 \leftarrow J$ transition frequencies calculated using the conformer's ground-state rotational constants requires SA and SG populations of 0.43 and 0.57, after correcting for the conformer's μ_a and transition frequency differences, to match the EA band frequency and $k_{iso} = 27$ GHz ($k_{SA\rightarrow SG} = 16$ GHz, $k_{SG\rightarrow SA} = 11$ GHz) to reproduce the EA bandwidth. Simulations using a three-site exchange mechanism require specification of the average rotational constants, μ_a, and population of the delocalized torsional states forming the third exchanging species, which can only be estimated from models, and the exchange rate constants among the three species. For example, the frequency and width of the EA band at 297 K is reproduced with equal signal intensities for the three exchanging species using the population-weighted averages of the scaled rotational constants for the D states: *A*/MHz = 6540, *B*/MHz = 1541, *C*/MHz = 1343 and $k_{SA\rightarrow SG} = k_{SA\rightarrow DLS} = k_{SG\rightarrow DLS} = 7$ GHz. These interdependent parameters can be varied over large ranges while producing similarly good simulations of the experimental spectrum. In all two- and three-site simulations that reproduce the EA band, the individual *K*-sublevel transitions are calculated to have Lorentzian line shape functions (before applying the Stark-modulation profiles) with widths ∼230 MHz (fwhm) that vary by less than 5%. This is a result of the fact that the frequency differences among the individual *K*-sublevel transitions are small compared to the frequency difference between the $J + 1 \leftarrow J = 10 \leftarrow 9$ SA and SG bands and because $\tau_{iso} \ll \tau_{sp}$. Simulations of the $11 \leftarrow 10$, $12 \leftarrow 11$, and $13 \leftarrow 12$ transitions at 297 and 210 K also show that the EA bands are insensitive to mechanistic information, and the lifetimes required to reproduce the bands result in

linewidths, which can also be reasonably attributed to the exchange-averaged rotational-constant distribution of the thermal sample.

Even though the EA bands are at fast exchange and it is not possible to obtain mechanistic information or definitive conformer lifetimes, it is possible to estimate upper-limit τ_{iso}'s and the maximum distribution of the exchange-averaged rotational-constant sum, $B + C$, of the population producing the EA bands. This was done by first estimating limits for the *K*-sublevel frequency dispersion for each band and then adjusting the linewidths of the *K*-sublevel transitions to match the observed band profiles. Linewidths were attributed to either exchange averaging to determine upper-limit τ_{iso}'s or to the rotational-constant distribution in the thermal sample to determine $\sigma(B + C)$, the standard deviation of the exchange-averaged rotational-constant sum $B + C$.

Upper-limit τ_{iso}'s were determined by attributing the width of the EA bands exclusively to *K*-sublevel structure and exchange averaging. A−E splittings were not considered to contribute significantly to the observed band widths of the EA series because A−E splittings were not observed in the high-resolution spectra of the SA and SG conformers of ECF, consistent with the 1192 cm^{-1} barrier to internal rotation of the methyl group for the SA conformer, calculated using the MP2/HF/6-311++G**. Methyl rotor torsional states above the 1200 cm^{-1} methyl internal rotation barrier provide an additional source of internal angular momentum and potential spectral broadening but they do not contribute significantly to the state density and this effect was not considered in the following analysis. The *K*-sublevel transition frequencies of nearly prolate molecules are determined by κ, $B + C$, and *J*. Spectral simulations of the EA bands used $\kappa = -0.923$ (the average of κ for the SA and SG conformers), which produces a frequency dispersion of the *K*-sublevel transitions included in the bands of ∼75 MHz at $J + 1 = 10$ and ∼120 MHz for $J + 1 = 13$. Using $\kappa = -0.923$ requires sets of rotational constants with $B + C = 2863$ MHz at 297 K and $B + C = 2861$ MHz at 210 K to reproduce the frequencies of the EA band series. Rotational constants used in all simulations at 297 K were: *A*/MHz = 6490.0, *B*/MHz = 1530.1, *C*/MHz = 1332.7. Rotational constants used in all simulations at 210 K were: *A*/MHz = 6483.0, *B*/MHz = 1528.8, *C*/MHz = 1331.1. (These rotational constants are slightly larger than the thermal average rotational constants for the eigenvalues of the O−ethyl torsional potential function calculated with the MP2/HF/6-311++G** model: *A*/MHz = 6617.2, *B*/MHz = 1527.4, *C*/MHz = 1318.1 at 210 K ($\kappa = -0.921$) and *A*/MHz = 6626.8, *B*/MHz = 1529.5, and *C*/MHz = 1322.8 at 297 K ($\kappa = -0.922$). Adjusting κ changes the frequency dispersion of the *K*-sublevel transitions and requires slightly different rotational constants to reproduce the frequencies of the EA bands. For example, reducing κ to −0.935 decreases the frequency dispersion of the *K*-sublevel transitions included in the pileups to 63 MHz, and increasing κ to −0.915 increases the frequency dispersion of the *K*-sublevel transitions to 87 MHz for the $J + 1 = 10$ transition. The width of the bands of the EA series are ∼3−4 times greater than the estimated *K*-sublevel width. Simulations used standard relative intensities of the *K*-sublevel transitions at 297 and 210 K.[14] The intensities of the *K*-sublevel transitions of the EA bands may be perturbed by *K*-sublevel mixing, which can result in exchange networks with averaged *K*-sublevel indices and transitions involving sublevels with low- and high-*K*-sublevel indices may be less intense or absent.

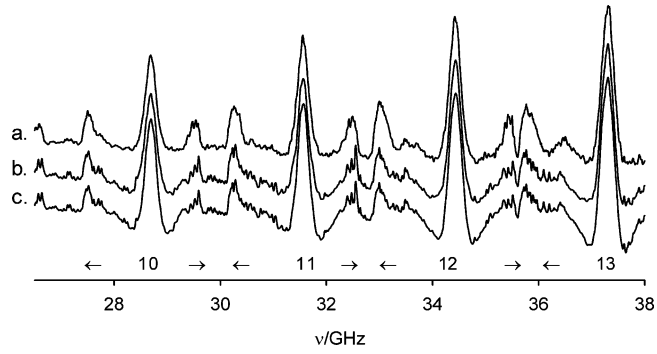

Figure 5. Comparison of the experimental rotational spectrum of ECF at 297 K with simulations; a, experimental spectrum; b, simulated spectrum with τ_{iso} values listed in Table 2; c, simulated spectrum assuming a normal distribution of the rotational-constant sum $B + C$ for the fraction producing the EA band series using parameters listed in Table 3. Sets of arrows (← $J + 1$ →) point to the $J + 1 \leftarrow J$ bands of the SA (←) and SG (→) conformers.

For each EA band, a Lorentzian line shape function was applied to each *K*-sublevel transition and its Stark lobes were calculated using the rotational constants listed above. The line width was the same for all of the *K*-sublevel transitions in the band. In the fast-exchange regime, the width of the Lorentzian lines for a given rate constant are determined by the frequency separation of the slow-exchange transitions, which average to produce the fast-exchange line. Two-site exchange produces the largest spread of exchange-averaged *K*-sublevel linewidths for a given exchange rate constant. For the $J + 1 = 10$ band, a rate constant of 27.5 GHz results in an average exchange broadened line width of 230 MHz with $\sigma = 12$ MHz for all of the *K*-sublevel transitions included in the band. Fitting all of the *K*-sublevel transitions with a single line width results in less than 5% error in the resulting rate constant for the $J + 1 = 10$ transition and less for the higher *J* transitions because the SA−SG frequency separations increase at a larger rate than sublevel dispersion increases. The simulated bands were compared to the observed and the Lorentzian line width applied to all of the *K*-sublevel transitions in each band was adjusted to obtain the best fit. The nonexchange simulated spectrum was added to the calculated EA series and the ratios of exchange to nonexchange were adjusted to obtain the final simulations shown in part b of Figure 5 and in Figure 6. Table 1 lists the linewidths (fwhm) and resulting rate constants and $\langle \tau_{iso} \rangle$'s at 210 and 297 K for $J + 1 \leftarrow J = 10 \leftarrow 9$ to $J + 1 \leftarrow J = 13 \leftarrow 12$. Rate constants were calculated from the relationship: $k = (\pi\delta\nu)/(2)[((\delta\nu)/(W))^2 - ((W)/(\delta\nu))^2 + 2]^{1/2}$. W, the width (fwhm) of the Lorentzian line applied to each *K* sublevel transition and $\delta\nu$, the frequency difference between the SA and SG bands for each $J + 1$ value, are listed in Table 1. This equation is valid for equally populated two-site exchange as used in NMR spectroscopy where equal conformer populations produce equal signal intensities at slow exchange.[12] Corresponding $J + 1 \leftarrow J$ transitions of the SA and SG conformers of ECF have almost equal signal intensities. The ratio of signal intensities for the same $J + 1 \leftarrow J$ transition of the set of localized SA states and the set of localized SG states, $(S_{SA})/(S_{SG}) = ((\mu_{a_{SA}})/(\mu_{a_{SG}}))^2(((B + C)_{SA})/((B + C)_{SG}))^2((\sum e^{-(E_{iSA})/(kT)})/(\sum e^{-(E_{iSG})/(kT)})) = 1.125/1$ at 210 K and 1.045/1 at 297 K. These ratios were calculated using the experimentally determined dipole moments and rotational constants and the relative energies of the localized torsional states of the O−ethyl torsional potential described in ref 1. There are equal numbers of bound SA and SG states of the O−ethyl torsional potential function for ECF. Although the composition

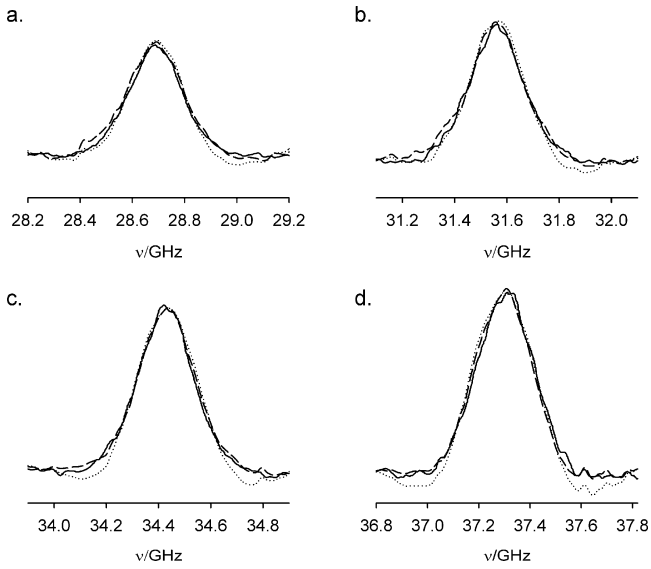

Figure 6. Simulations of EA bands of ECF at 297 K. Solid lines are experimental bands, dashed lines are simulated with Lorentzian line shape functions applied to the *K*-sublevel transitions and associated Stark lobes using parameters listed in Table 1, as described in the text. Dotted lines are simulations with Gaussian line shape functions applied to the *K*-sublevel transitions and associated Stark lobes using parameters listed in Table 2; a, $J + 1 \leftarrow J = 10 \leftarrow 9$; b, $J + 1 \leftarrow J = 11 \leftarrow 10$; c, $J + 1 \leftarrow J = 12 \leftarrow 11$; d, $J + 1 \leftarrow J = 13 \leftarrow 12$.

of individual exchange networks can vary, the signal intensity of sets of SA and SG states of exchange networks at high state density will approach these ratios. This method yields an upper limit for $\langle\tau_{iso}\rangle$ because the contribution due to scatter in the fast-exchange rotational constants in the thermal distribution is neglected in this analysis. Scatter in fast-exchange rotational constants reduces the line-width contribution from exchange and reduces the corresponding upper-limit $\langle\tau_{iso}\rangle$ required to simulate the EA bands.

The lower relative intensity of the EA series at 210 K made it difficult to determine linewidths from the complete spectral simulations because the EA bands overlap with transitions from the slow-exchange spectrum of the T and D states, which are not reproduced accurately. To determine the Lorentzian linewidths of the *K*-sublevel transitions at 210 K, the EA band simulations were compared to the experimental bands at 210 K without the inclusion of the slow-exchange contribution to the simulated spectrum. These simulations are shown in Figure 8. Figure 7 shows the total simulations at 210 K, which include the EA series and the slow-exchange spectrum.

Simulations with $\kappa = -0.92$ and $\kappa = -0.93$ were also performed. Using a set of rotational constants with $\kappa = -0.93$ requires 10−15 MHz increases in linewidths to reproduce the observed spectrum, consistent with 5−7% longer upper-limit $\langle\tau_{iso}\rangle$'s. In the extreme case where the width of the *K*-sublevel dispersion is reduced to zero ($\kappa = -1$) and the observed bands are assumed to be entirely due to lifetime broadening, upper-limit $\langle\tau_{iso}\rangle$'s are 20−25% longer than those listed in Table 1.

The EA band series can also be simulated assuming that conformer exchange is at the fast-exchange limit and the width is due only to rotational-constant scatter, which produces a distribution of weak, narrow (∼1 MHz) Lorentzian lines for each *K*-sublevel transition. To estimate the scatter, a Gaussian distribution was assumed and EA bands were simulated with Gaussian functions centered at each *K*-sublevel transition and its associated Stark lobes, and the width was adjusted to reproduce the observed bands. These simulations used the same sets of rotational constants at 210 and 297 K described above. Part c of Figures 5, Figure 6, part c of Figure 7, and Figure 8 show these simulations. The linewidths used and the σ values obtained are listed in Table 2. For nearly prolate ECF, the quantity, $\sigma/(J + 1)$ is approximately equal to $\sigma(B + C)$.

Simulations of the $J + 1 = 10-13$ EA bands indicate $\langle\tau_{iso}\rangle < \sim 40$ ps and $\sigma(B + C) < 12$ MHz for the population producing the EA band series. Comparisons of the Lorentzian and Gaussian line shape simulations and the observed spectra indicate that the Lorentzian lineshapes provides a marginally better fit. Lack of agreement near the baseline can also be due to a skewed *K*-sublevel intensity distribution resulting from *K*-sublevel averaging.

The population ratio *P*(slow exchange):*P*(EA) consistent with the experimental spectrum is 1:0.58(5) at 210 K and 1:2.33(1) at 297 K. This ratio was determined by adjusting the proportions of the calculated slow-exchange spectrum and the calculated EA band series using both Gaussian and Lorentzian linewidths listed in Tables 1 and 2. Simulated spectra with intensities calculated from these population ratios are shown in Figures 5 and 7. The average μ_a of the SA and SG conformers was used to calculate intensities of the EA band series. The *P*(slow exchange):*P*(EA)ratio for each $J + 1 \leftarrow J$ transition was determined separately from the integrated intensities of the unmodulated spectra used to calculate the Stark-modulated spectra. This was necessary because many Stark lobes and zero-field lines are overlapped in the cluttered spectra and the broad EA bands overlap with some of their own broadened Stark lobes. The Stark lobes for each transition with $K_p \geq 3$ extend over a 2 GHz frequency range due to the large *a* axis dipole moment and the high Stark field employed. Comparing the unmodulated intensity to the Stark-modulated intensities shows that the broader EA bands lose more intensity on modulation than the SA and SG bands. The entire spectrum can be simulated with one population ratio at each temperature, indicating that there is not a significant *J* dependence to the population producing the EA band.

The *P*(slow exchange):*P*(EA) ratios required to simulate the observed Stark-modulated R-band spectra of ECF can be compared to the vibrational population of ECF at 210 and 297 K. Figure 9 shows the vibrational energy distribution function for ECF at 210 and 297 K, which was obtained by multiplying the vibrational state density, $\rho(E)$, by the corresponding Boltzmann factor. The *P*(slow exchange):*P*(EA) ratios are consistent with the calculated ratio of the population below ∼700 cm^{-1} to the population above ∼700 cm^{-1}, *P*(<700 cm^{-1}):*P*(>700 cm^{-1}), of 1:0.48 at 210 K and 1:2.06 at 297 K. (The SA−SG barrier calculated using the MP2/HF/6-31++G** theoretical model is ∼360 cm^{-1}.) This result agrees with previously reported results for the $J + 1 \leftarrow J = 8 \leftarrow 7$ transition of ECF.[1]

Discussion

Attributing the entire width of the bands of the EA series to conformer exchange averaging and *K*-sublevel dispersion yields the upper-limit conformer lifetimes listed in Table 2. Calculated energy specific rate constants, $k(E)_{RRKM}$, for the SA−TS process of ECF were reported previously.[1] The thermal average RRKM rate constant, $\langle k(E)_{RRKM}\rangle$, of the population above 700 cm^{-1} is 301 GHz ($\langle\tau_{iso}\rangle$ = 3.32 ps) at 210 K and 325 GHz ($\langle\tau_{iso}\rangle$ = 3.08 ps) at 297 K. These rate constants are directly comparable to the k_{iso}'s reported in Table 2.[24] The RRKM rate constants are larger than the lower-limit rate constants determined for the $J + 1 = 10$, 11, 12, and 13 bands by approximately 1 order of magnitude. The calculated $\langle k(E)_{RRKM}\rangle$'s would produce lifetime-

TABLE 1: Lower-Limit Isomerization Rate Constants, $\langle k(E)\rangle$ and Upper-Limit Conformer Lifetimes, $\langle\tau_{iso}\rangle$, for SA−SG Conformer Exchange of ECF at 297 and 210 K[a]

$J+1$	$\nu_{SG}-\nu_{SA}$/MHz	fwhm/ MHz 297 K	lower-limit $\langle k(E)\rangle$/ GHz 297 K	upper-limit $\langle\tau_{iso}\rangle$/ ps 297 K	fwhm/ MHz 210 K	lower-limit $\langle k(E)\rangle$/ GHz 210 K	upper-limit $\langle\tau_{iso}\rangle$/ ps 210 K
10	1995	230	27.5	36.3	260	24.5	40.9
11	2190	250	30.5	32.8	290	26.4	37.8
12	2405	300	30.7	32.5	320	28.9	34.6
13	2695	340	34.1	29.3	360	32.2	31.0

[a] $\nu_{SG}-\nu_{SA}$ is the frequency difference of the SG and SA conformer bands for each $J+1 \leftarrow J$ transition and FWHM is the full width at half maximum of the Lorentzian lineshape applied to each $J'_{K_p'K_o'} \leftarrow J''_{K_p''K_o''}$ transition and its Stark lobes in the simulated EA band. $\langle k(E)\rangle$ was calculated as described in the text. Simulations are shown in Figures 6 and 8.

TABLE 2: Gaussian Linewidths Simulation Parameters[a]

$J+1$	fwhm/MHz 297 K	σ/MHz 297 K	$\sigma/(J+1)$ MHz 297 K	fwhm/MHz 210 K	σ/MHz 210 K	$\sigma/(J+1)$ MHz 210 K
10	210	89.2	8.9	250	106.2	10.6
11	235	99.8	9.1	280	118.9	10.8
12	285	121	10.1	310	131.6	11.0
13	305	129	9.9	350	148.6	11.4

[a] FWHM is the full width at half maximum applied to each $J'_{K_p'K_o'} \leftarrow J''_{K_p''K_o''}$ transition and its Stark lobes for each simulated EA band. Simulations are shown in Figures 6 and 8.

TABLE 3: Averages and Standard Deviations of the Rotational-Constant Sum, $B+C$ for the population above 700 cm^{-1} of ECF with $J=10$[a]

	$\langle B+C\rangle$/MHz	$\sigma(B+C)$/MHz
	Model a	
210 K	2852.6	50.9
297 K	2854.5	46.9
	Model b	
210 K	2857.1	12.0
297 K	2858.2	11.4

[a] Model a.: Exchange networks extend over 1 cm^{-1} and consist of zero-order states with $10_{0\ 10}$ rotational energy level. Model b.: Exchange networks extend over 1 cm^{-1} and contain all possible K-sublevels for $J=10$. For each 1 cm^{-1} exchange network, $B+C$ was calculated according to: $B+C = F_{SA}\cdot\langle B+C\rangle_{SA} + F_{SG}\cdot\langle B+C\rangle_{SG} + F_D\cdot(B+C)_D + F_T\cdot(B+C)_T$ and the population fraction for each energy grain F_i was determined from the state densities shown in Figure 10.

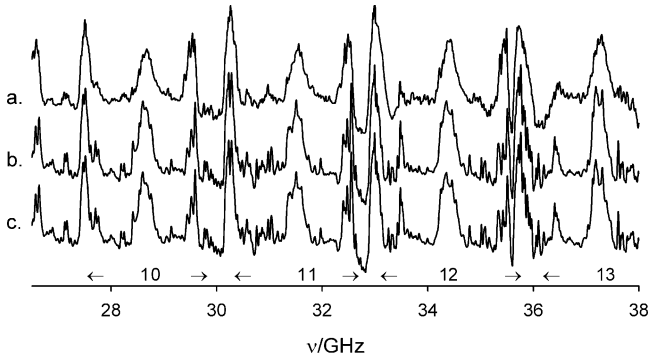

Figure 7. Comparison of experimental rotational spectrum of ECF at 210 K with simulations; a, experimental spectrum; b, Lorentzian simulation; c, Gaussian simulation. Sets of arrows (← $J+1$ →) point to the $J+1 \leftarrow J$ bands of the SA (←) and SG (→) conformers.

broadened linewidths of only ∼20 MHz for the K-sublevel transitions of the $J+1 \leftarrow J=10 \leftarrow 9$ transition and ∼40 MHz for the $J+1 \leftarrow J=13 \leftarrow 12$. The observed EA series bandwidths would only be consistent with the calculated $\langle k(E)_{RRKM}\rangle$'s if the distribution of exchange-averaged rotational constants was responsible for the additional width.

Upper-limit conformer isomerization lifetimes of the thermal population of ECF can be compared with previous work. A

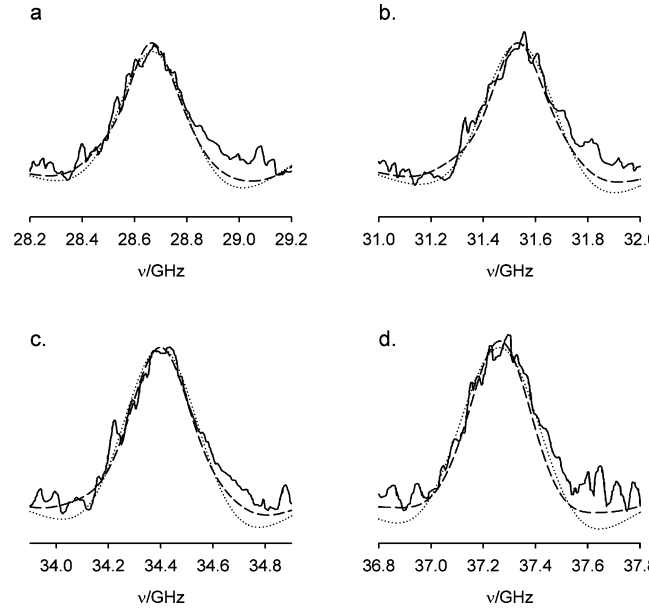

Figure 8. Simulations of EA bands of ethyl cyanoformate at 210 K. Solid lines are experimental bands, dashed lines are simulated with Stark-modulated Lorentzian lines applied to the K-sublevel structure with parameters listed in Table 1 as described in the text. Dotted lines are simulations with Stark-modulated Gaussian linewidths applied to the K-sublevel structure with parameters listed in Table 2; a, $J+1 \leftarrow J=10 \leftarrow 9$; b, $J+1 \leftarrow J=11 \leftarrow 10$; c, $J+1 \leftarrow J=12 \leftarrow 11$; d, $J+1 \leftarrow J=13 \leftarrow 12$.

conformer lifetime of ∼170 ps was recently determined from analysis of the $2_{02} \leftarrow 1_{01}$ rotational transition of cyclopropane carboxaldehyde molecules with ∼2800 cm^{-1} of vibrational energy. The syn and anti conformers of cyclopropane carboxaldehyde are separated by a barrier of ∼1910 cm^{-1}, the total vibrational state density of cyclopropane carboxaldehyde is ∼50 states/cm^{-1} at 2800 cm^{-1}, and the lifetime determined is ∼16 times slower than predicted using RRKM theory.[5a] A ∼25 ps conformer lifetime for pentenyne with ∼3330 cm^{-1} of vibrational energy was also obtained by analysis of the $2_{02} \leftarrow 1_{01}$ rotational transition.[5b] The conformer isomerization barrier for pentenyne is ∼1000 cm^{-1}, the total vibrational state density near 3330 cm^{-1} is ∼800/ cm^{-1}, and the observed lifetime is ∼50 times longer than predicted using RRKM theory. When coherent state preparation is used, the conformer lifetime of pentenyne

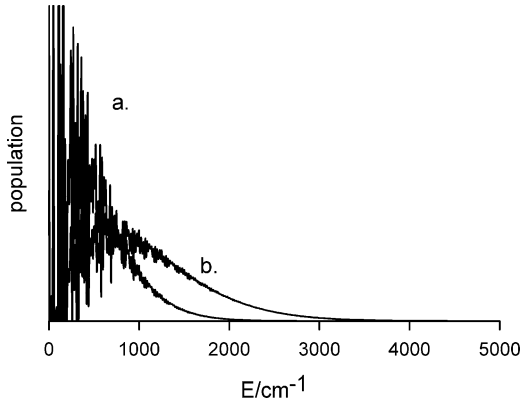

Figure 9. Vibrational energy distribution function for ECF at: a, 210 K; and b, 297 K.

is ~1200 ps at comparable vibrational energies. Recent advances in vibrational spectroscopy make it possible to determine conformer lifetimes for molecules undergoing low-barrier conformational processes in thermally equilibrated condensed phase samples. In condensed phase samples, the time scales for conformer exchange and intermolecular energy exchange are competitive. The lifetime for the gauche ↔ trans isomerization, τ_{iso} of ethyl isocyanate in 2-methylpentane solution, determined from analysis of ultrafast vibrational echo experiments, is only 2.2 ps at 298 K and 90 ps at 110 K. The temperature dependence of τ_{iso} is consistent with an isomerization barrier of ~400 cm^{-1}.[25] The lifetime for the gauche−trans isomerization of 1-fluoro-2-isocyanato-ethane in CCl_4 at room temperature, obtained using 2D vibrational echo spectroscopy, is 43(10) ps at 298 K,[4,26] comparable to upper-limit conformer lifetimes obtained in the present study.

Attributing the EA bandwidths to *K*-sublevel dispersion and the thermal $B + C$ distribution yields $\sigma(B + C) = \sim 12$ MHz. The exchange network model described in the introduction section was used to estimate the thermal distribution of exchange network-averaged rotational constants. The scatter of the properties of the thermal distribution of exchange networks depends on the number of rovibrational states included in each exchange network. The magnitude of coupling terms that could be used to estimate the size and energy spread of the exchange networks is not known. For comparison purposes, exchange networks were assumed to consist of all of the states within 1 cm^{-1} energy grains with equal mixing coefficients and exchange network properties were calculated at 1 cm^{-1} intervals. Two models were used: Model a, restricted exchange networks to rovibrational states with the same J and K values in a 1 cm^{-1} energy range; Model b, restricted exchange networks to rovibrational states with the same J value independent of the K sublevel indices. Rovibrational state densities for the $J_{K_pK_o} = 10_{0\ 10}$ rotational level and for all possible rotational levels for $J = 10$ were used to determine the spectral consequences of Model a and Model b, respectively. State densities were calculated as described previously but included rotational energy levels of each zero-order vibrational state.[1] Vibrational state densities were calculated using the Stein−Rabinovitch extension of the Beyer−Swinehart algorithm.[27] Troe's approximation[28] was used to evaluate the contribution for the methyl top rotor using the barrier calculated at the MP2/6-311++G** theory level, 1192 cm^{-1}. The $C(sp^2)$−O(ether) torsion was included as a vibration with $\nu =$ 113.9 cm^{-1}. The energies of the O−ethyl torsional states shown in Figure 4 were used directly. All other vibrational frequencies used were calculated at the HF/6-311++G** level and scaled by a factor of 0.88. The zero-order vibrational states were

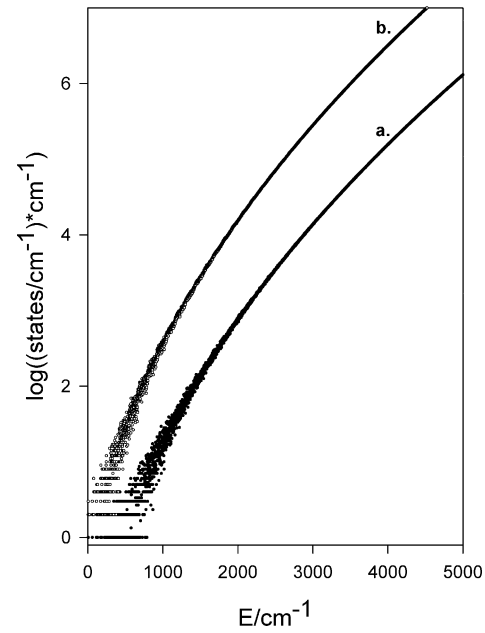

Figure 10. Total rovibrational state densities of ECF for $J = 10$; a, only $10_{0,10}$ rotational state included; b, all 21 *K*-sublevels of $J = 10$ are included.

separated into four groups: SA, SG, T, and D based on their O−ethyl torsional quantum numbers as described above and shown in Figure 4 and rovibrational state densities were calculated separately for each set. Rotational energy levels were calculated using the experimentally determined rotational constants of the SA and SG conformers and the average of the SA and SG rotational constants were used for the T and D states. State densities and all subsequent calculations where they were used were calculated up to 10 000 cm^{-1}. The rovibrational state density for $J = 10$ is shown in Figure 10. The lower and upper plots are for Models a and b, respectively. The rovibrational state density near 360 cm^{-1}, the MP2/HF/6-311++G** SA−SG conformer barrier, is ~1/cm^{-1} for Model a and ~20/cm^{-1} for Model b. At 700 cm^{-1}, the rovibrational state density increases to ~4/cm^{-1} for Model a and ~100/cm^{-1} for Model b. The grain composition of 1 cm^{-1} energy grains for Models a and b are shown in parts a and b of Figure 11, respectively. *F*s are fractions of zero-order states identified as SA, SG, D, or T based on their O−ethyl torsional quantum numbers. Both models predict large scatter in grain composition at lower energies with many empty grains. For Model a, the majority of 1 cm^{-1} energy grains between 360 cm^{-1} and 700 cm^{-1} do not contain both SA and SG states and therefore cannot undergo conformer exchange averaging. For Model b, approximately half of the 1 cm^{-1} grains between 360 and 700 cm^{-1} contain both SA and SG states but there are large fluctuations in composition and exchange networks with these grain compositions would not have the similar fast-exchange rotational constants required to produce a narrow exchange-averaged band series. For both models, the grain composition becomes more uniform at higher energies as the number of states in each grain increases. The grain composition does however change slowly with energy because the number of accessible D states increases with energy, whereas the number of accessible SA, SG, and T states are all fixed at 6.

Grain-averaged rotational constants were calculated as a function of energy for 1 cm^{-1} energy grain sizes for both models. The fast-exchange-averaged $B + C$ value of each energy grain was calculated from the fractional composition of the grain: $\langle B$

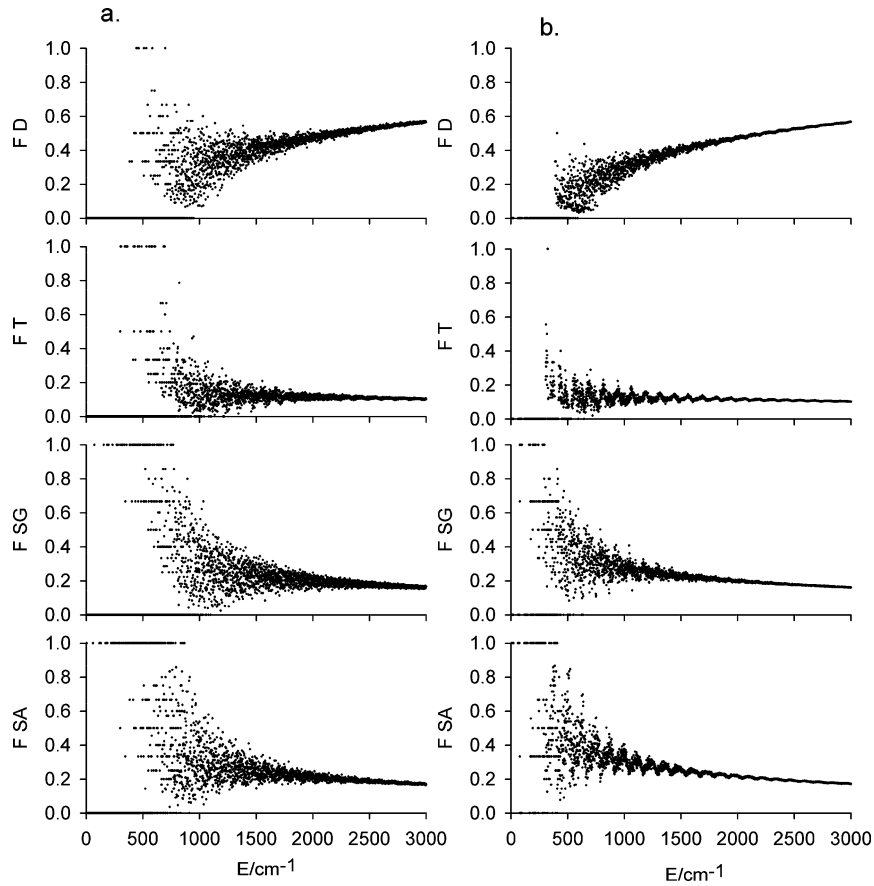

Figure 11. Fractional composition of 1 cm^{-1} energy grains as a function of total vibrational energy for $J = 10$. Zero-order rovibration states are grouped based on the number of quanta in the O−ethyl torsion. Groups are designated SA (syn−anti, there are six SA states with wave functions localized in the syn−anti well), SG (syn−gauche, there are six states with wave functions localized in the syn−gauche well). T (six states near the SA−SG barrier) and D (delocalized states above the SA−SG barrier). a. Model a, exchange networks composed of rovibrational states with 10_{010} rotational level only. b. Model b, all *K*-sublevels for $J = 10$ are included in exchange networks.

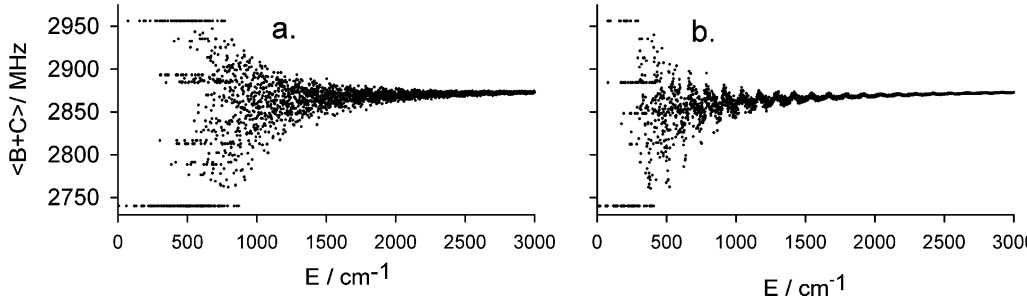

Figure 12. The average $B + C$ of 1 cm^{-1} energy grains as a function of rovibrational energy for ECF with $J = 10$. $B + C$ was determined from $B + C = F_{SA}\cdot\langle B + C\rangle_{SA} + F_{SG}\cdot\langle B + C\rangle_{SG} + F_D\cdot\langle B + C\rangle_D + F_T\cdot\langle B + C\rangle_T$, where the fractions *F*s are shown in Figure 11 and the $\langle B + C\rangle$'s are listed in the text. a. Model a, only $10_{0\ 10}$ sublevel included; b. Model b, all *K*-sublevels for $J = 10$ included.

$+ C\rangle = F_{SA}\cdot\langle B + C\rangle_{SA} + F_{SG}\cdot\langle B + C\rangle_{SG} + F_{TS}\cdot\langle B + C\rangle_{TS} + F_D\cdot\langle B + C\rangle_D$ with $\langle B + C\rangle_{SA} = 2740$ MHz, $\langle B + C\rangle_{SG} = 2956$ MHz, $\langle B + C\rangle_{TS} = 2893$ MHz, and $\langle B + C\rangle_D = 2885$ MHz. These are the average of the scaled $B + C$ values of the O−ethyl torsional states consistent with the potential function calculated using the MP2/HF/6-311++G** theoretical model described previously. The energy dependence of the average $B + C$ value for 1 cm^{-1} energy grains for both Models is shown in Figure 12. The $B + C$ value required to reproduce the experimental frequencies of the EA series, 2863 MHz, is larger than the average of the $B + C$ values of the SA and SG conformationally localized states, which have almost equal populations and dipole moments. When all of the states are included in the average, the calculated $B + C$ is larger and closer to the observed value. The shift to larger $B + C$ with increasing energy shown in Figure 12 occurs because the number of delocalized states increases with energy, whereas the number of SA, SG, and T states is fixed.[29]

Both models predict large scatter in fractional composition and energy grain average $B + C$ values at low energies. The $B + C$ scatter predicted by Model a is not consistent with formation of intense EA band unless the actual exchange networks at lower energies consist of more states and encompass much larger energy ranges ∼10−20 cm^{-1}. Model b is consistent with the small scatter required for formation of the EA band by exchange networks above 700 cm^{-1}.

The distribution of the rotational-constant sum, $B + C$, of the population above 700 cm^{-1} at 210 and 297 K is shown in Figure 13. The fraction of the total population contained in each 1 cm^{-1} energy grain, $F_i = (\rho(E)_i e^{-E_i/kT})/(\sum\rho(E)_j e^{-E_j/kT})$, and the

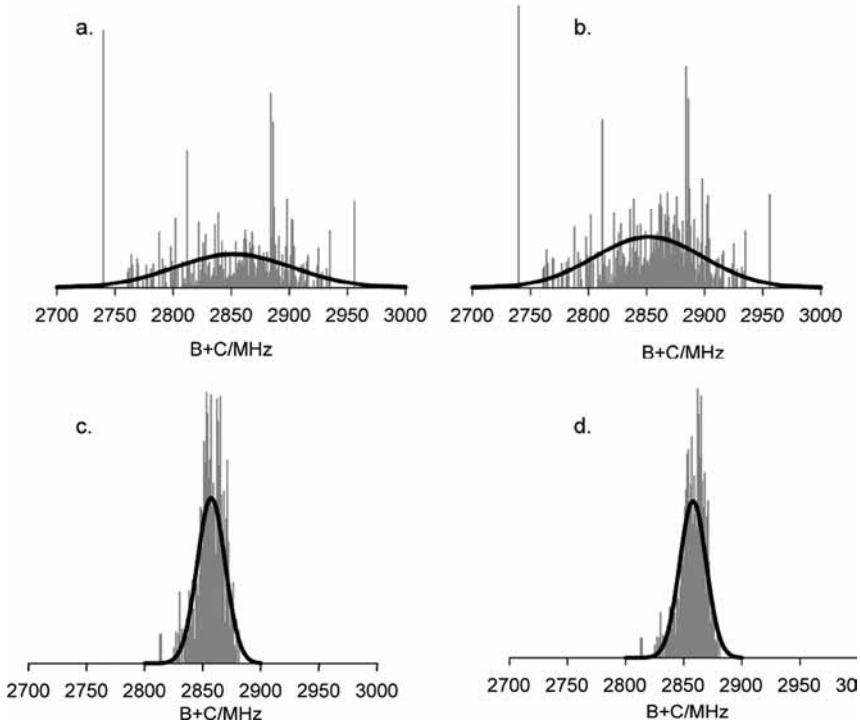

Figure 13. Distributions of the rotational-constant sum, $B + C$, for the thermal population with $J = 10$ at 210 and 297 K. Fractional populations of the energy grains were determined from the rovibrational state densities shown in Figure 10 using a Boltzmann distribution and $B + C$ for each grain is shown in Figure 12. a. Model a, only $10_{0\,10}$ sublevel included, 210 K; b. Model a, only the $10_{0\,10}$ K-sublevel is included, 297 K; c. Model b, all K-sublevels for $J = 10$ included, 210 K; d. Model b, all K-sublevels for $J = 10$ included, 297 K. Solid lines are normal distribution functions calculated with the parameters listed in Table 3.

average $\langle B + C \rangle_i$ of each grain were used to estimate the thermal average $B + C$ and its standard deviation, which are listed in Table 3. For Figure 13, the population with $B + C$ within 1 MHz intervals was plotted for clarity. Solid lines correspond to a normal distribution using the σ values and average $B + C$ values listed in Table 3. Model a predicts a frequency distribution for the sublevel transitions of the $J + 1 \leftarrow J = 10 \leftarrow 9$ EA band of over 1 GHz at 210 and 297 K. Model b predicts a frequency distribution for the sublevel transitions of ~500 MHz at 210 K and ~275 MHz at 297 K for the $J + 1 \leftarrow J = 10 \leftarrow 9$ close to the observed upper limit. Model a attains a comparable state density and $B + C$ distribution at about twice the internal energy, 1500 cm^{-1}. The fraction of the population with energy above 1500 cm^{-1} is 0.02 at 210 K and 0.23 at 297 K and is not consistent with the intense EA bands observed. Exchange networks consisting of only zero-order states with the same K-sublevel indices would have to extend over energy intervals greater than 20 cm^{-1} to produce the population and $B + C$ distribution observed.

Conclusions

Rotational spectra of ECF at 210 and 297 K are not consistent with slow conformer exchange ($\tau_{iso} \gg \tau_{sp}$ where $\tau_{sp} > 400$ ps). Three possible interpretations are consistent with the width and temperature dependence of the EA bands. 1. The width is exclusively the result of lifetime broadening. In this case, upper-limit conformer lifetimes are ~1 order of magnitude longer than RRKM predictions and decrease with increasing J. 2. The spectrum is at the fast-exchange limit ($\tau_{iso} \ll \tau_{sp}$) and the width of the EA bands is due to the thermal distribution of exchange-averaged rotational constants. Model calculations demonstrate for this to occur in the population fraction consistent with the relative intensity of the EA series; states with different K-sublevel indices must be included in exchange networks or the energy span of zero-order states in each exchange network must extend over several cm^{-1}. 3. Both lifetime broadening and the rotational-constant distribution contribute to the width of the EA series bands. This requires $\langle \tau_{iso} \rangle$ to be shorter than the upper-limit values listed in Table 1 and closer to the RRKM predictions and the rotational-constant distribution to be smaller than the values listed in Table 2. In this case, the rotational-constant distribution can only partially account for the increase in bandwidth with increasing J and $\langle \tau_{iso} \rangle$ must have a small J dependence.

Acknowledgment. We thank the National Science Foundation (Grant # NSF CHE 0643719) for support of this research.

References and Notes

(1) True, N. S. *J. Phys. Chem. A* **2006**, *110*, 7364–7374.

(2) True, N. S., Bohn, R. K. *Paper T106*, 61st International Symposium on Molecular Spectroscopy, Ohio State University, June 2006.

(3) True, N. S. Bohn, R. K. *Paper R109*, 61st International Symposium on Molecular Spectroscopy, Ohio State University, June 2006.

(4) Zheng, J.; Kwak, K.; Fayer, M. D. *Science* **2006**, *313*, 1951–1955.

(5) (a) Dian, B. C.; Brown, G. G.; Douglass, K. O.; Pate, B. H. *Science* **2008**, *320*, 924–928. (b) Dian, B. C.; Brown, G. G.; Douglass, K. O.; Rees, F. S.; Johns, J. E.; Nair, P.; Suenram, R. D.; Pate, B. H. *Proc. Natl. Acad. Sci. U.S.A.* **2008**, *105*, 12696–12700.

(6) Keske, J.; McWhorter, D. A.; Pate, B. H. *Int. Reviews in Physical Chemistry* **2000**, *19*, 363–407.

(7) Keske, J. C.; Pate, B. H. *Annu. Rev. Phys. Chem.* **2000**, *51*, 323–353.

(8) (a) Pate, B. H. *J. Chem. Phys.* **1998**, *109*, 4396–4406. (b) Pate, B. H. *J. Chem. Phys.* **1999**, *110*, 1990–1999.

(9) Kubo, R. In *Fluctuation, Relaxation and Resonance in Magnetic Systems*; Haar, D. T., ed.; Oliver and Boyd Ltd.: Edinburgh, 1962; p 23.

(10) (a) MacPhail, R. A.; Strauss, H. L. *J. Chem. Phys.* **1985**, *82*, 1156–1166. (b) Wood, K. A.; Strauss, H. L. *J. Phys. Chem.* **1990**, *94*, 5677–5684.

(11) *Dynamic Nuclear Magnetic Resonance Spectroscopy*, Jackman, L. M., Cotton, F. A., eds.; Academic Press: New York, 1975.
(12) Sandström, J. *Dynamic NMR Spectroscopy*; Academic Press, New York, 1982.
(13) Farag, M. S.; Bohn, R. K. *J. Chem. Phys.* **1975**, *62*, 3946–3950.
(14) Gordy, W.; Cook, R. L. *Microwave Molecular Spectra (Techniques of Chemistry)*, 3rd ed.; John Wiley and Sons, Inc.: New York, 1984.
(15) True, N. S.; Bohn, R. K. *J. Am. Chem. Soc.* **1976**, *98*, 1188–1194.
(16) Bohn, R. K.; Farag, M. S.; Ott, C. M.; Radhakrishnan, J.; Sorenson, S. A.; True, N. S. *J. Mol. Struct.* **1992**, *268*, 107–121.
(17) Ortigosa, J.; Hougen, J. T. *J. Chem. Phys.* **2000**, *112*, 10212–10220.
(18) Ortigosa, J. *Phys. Rev. A* **1996**, *179*, 41.
(19) Keske, J. C.; Rees, F. S.; Suenram, R. D.; Pate, B. H. *Phys. Chem. Chem. Phys.* **2003**, *5*, 1599–1609.
(20) McIlroy, A.; Nesbitt, D. A. *J. Chem. Phys.* **1994**, *101*, 3421–3435.
(21) McWhorter, D. A.; Hudspeth, E.; Pate, B. H. *J. Chem. Phys.* **1999**, *110*, 2000–2009.
(22) McWhorter, D. A.; Pate, B. H. *J. Mol. Spectrosc.* **1999**, *193*, 159–165.
(23) Suenram, R. D.; True, N. S.; Bohn, R. K. *J. Mol. Spectrosc.* **1978**, *69*, 435–444.
(24) The measured isomerization rate constant, $k_{iso} = k_{SA\rightarrow SG} + k_{SG\rightarrow SA} \cong 2k_{SA\rightarrow SG}$ because the SA and SG populations are almost equal and $k_{SA\rightarrow TS} = 2k_{SA\rightarrow SG}$.
(25) Levinger, N. E.; Davis, P. H.; Behere, P. K.; Meyers, D. J.; Stromberg, C.; Fayer, M. D. *J. Chem. Phys.* **2003**, *118*, 1312–1326.
(26) Finkelstein, I. J.; Zheng, J.; Ishikawa, H.; Kim, S.; Kwak, K.; Fayer, M. D. *Phys. Chem. Chem. Phys.* **2007**, *9*, 1533–1549.
(27) Holbrook, K. A.; Pilling, M.; Robertson, S. H. *Unimolecular Reactions*, Second ed.; John Wiley and Sons: NY, 1996.
(28) Troe, J. *J. Chem. Phys.* **1977**, *66*, 4758.
(29) The oscillation of the fractional composition and $B + C$ value at $\sim$70 cm^{-1} energy intervals shown in Figures 10 and 11 occurs because the SA conformer's four lowest calculated vibrational frequencies, 64.4, 113.9, 126.3, and 241.5 cm^{-1}, are almost integer multiples of each other and form clusters of higher state density separated by regions of low state density. This feature is more dramatic when the 21 rotational levels for $J = 10$, which span $\sim$20 cm^{-1} are included in the calculations (Model b). The lowest four calculated vibrational frequencies of the SG conformer, 66.4, 93.6, 160.7, and 218.8 cm^{-1}, do not produce as pronounced clusters of states.

JP902619K